Neoplasia 36 (2023) 100872

Contents lists available at ScienceDirect

Neoplasia

journal homepage: www.elsevier.com/locate/neo

Original Research

# Subclonal evolution and expansion of spatially distinct THY1-positive cells is associated with recurrence in glioblastoma

Wajd N. Al-Holou[a,1], Hanxiao Wang[b,e,1], Visweswaran Ravikumar[d], Sunita Shankar[a], Morgan Oneka[d], Ziad Fehmi[a], Roel GW Verhaak[g], Hoon Kim[g,h], Drew Pratt[c], Sandra Camelo-Piragua[c], Corey Speers[b], Daniel R Wahl[b], Todd Hollon[a], Oren Sagher[a], Jason A Heth[a], Karin M. Muraszko[a], Theodore S. Lawrence[b], Ana C de Carvalho[f], Tom Mikkelsen[f], Arvind Rao[b,d], Alnawaz Rehemtulla[b,*]

[a] Department of Neurosurgery, University of Michigan, Ann Arbor, MI 48109, United States
[b] Department of Radiation Oncology, University of Michigan, NCRC 520, Room 1342, Ann Arbor, MI 48105, United States
[c] Department of Pathology, University of Michigan, United States
[d] Department of Computational Medicine & Bioinformatics, The University of Michigan Medical School, Ann Arbor, MI 48109, United States
[e] AstraZeneca, United States
[f] Department of Neurosurgery, Henry Ford Hospital, Detroit, MI 48202, United States
[g] The Jackson Laboratory, Farmington, CT 06032, United States
[h] Department of Biopharmaceutical Convergence, Sungkyunkwan University, South Korea

ARTICLE INFO

*Keywords:*
Subclonal evolution
Treatment resistance
Glioblastoma

ABSTRACT

*Purpose:* Glioblastoma(GBM) is a lethal disease characterized by inevitable recurrence. Here we investigate the molecular pathways mediating resistance, with the goal of identifying novel therapeutic opportunities.
*Experimental design:* We developed a longitudinal *in vivo* recurrence model utilizing patient-derived explants to produce paired specimens(pre- and post-recurrence) following temozolomide(TMZ) and radiation(IR). These specimens were evaluated for treatment response and to identify gene expression pathways driving treatment resistance. Findings were clinically validated using spatial transcriptomics of human GBMs.
*Results:* These studies reveal in replicate cohorts, a gene expression profile characterized by upregulation of mesenchymal and stem-like genes at recurrence. Analyses of clinical databases revealed significant association of this transcriptional profile with worse overall survival and upregulation at recurrence. Notably, gene expression analyses identified upregulation of *TGFβ* signaling, and more than one-hundred-fold increase in *THY1* levels at recurrence. Furthermore, THY1-positive cells represented <10% of cells in treatment-naïve tumors, compared to 75-96% in recurrent tumors. We then isolated THY1-positive cells from treatment-naïve patient samples and determined that they were inherently resistant to chemoradiation in orthotopic models. Additionally, using image-guided biopsies from treatment-naïve human GBM, we conducted spatial transcriptomic analyses. This revealed rare *THY1*+ regions characterized by mesenchymal/stem-like gene expression, analogous to our recurrent mouse model, which co-localized with macrophages within the perivascular niche. We then inhibited TGFBRI activity *in vivo* which decreased mesenchymal/stem-like protein levels, including THY1, and restored sensitivity to TMZ/IR in recurrent tumors.
*Conclusions:* These findings reveal that GBM recurrence may result from tumor repopulation by pre-existing, therapy-resistant, THY1-positive, mesenchymal cells within the perivascular niche.

## Introduction

Glioblastoma (GBM), the most common primary intraparenchymal brain tumor, is a lethal disease with a median survival of 15 months that is characterized by treatment resistance, aggressive brain invasion, and inevitable recurrence, with less than 10% of patients surviving beyond 5 years [1,2]. A major obstacle contributing to rapid recurrence and the lack of effective treatments is the marked intra- and inter-tumoral heterogeneity in GBM [3–6]. Furthermore, given the heterogeneity present within GBM, it has been postulated that evolution and

* Corresponding author.
*E-mail address:* alnawaz@med.umich.edu (A. Rehemtulla).
[1] Contributed Equally.

https://doi.org/10.1016/j.neo.2022.100872
Received 19 December 2022; Accepted 22 December 2022

expansion of pre-existing treatment-resistant sub-clones are often responsible for inevitable recurrence [5,7,8]. Intratumoral heterogeneity can be seen at both at the cellular and microenvironmental level. At the tumor microenvironmental level, distinct niches, especially perivascular, hypoxic, and invasive tumor niches, have been shown to be enriched with therapy-resistant cancer stem cell (CSC) populations, also described as recurrence-initiating stem cells [3,7,9,10]. These pre-existing CSC populations are thought to play a critical role in driving treatment resistance and are characterized by self-renewal, differentiation, and the ability to expand and repopulate tumors post-therapy [11]. Definitive evidence for the role for pre-existing treatment-resistant cancer stem cells in evading chemo-radiation therapy as well as the mechanistic basis for this phenotype is lacking. An understanding of the genetic basis and gene expression changes driving the therapy resistant phenotype should provide an opportunity for therapeutic intervention to decrease the recurrence rate in GBM.

In this effort, we have utilized a longitudinal mouse model developed using patient-derived GBM explants to recapitulate the clinical treatment paradigm. Using this model, we generated pre-treatment and recurrent paired samples from each experimental mouse with the goal of identifying differentially expressed genes that should provide a molecular basis for tumor recurrence. Systematic analyses of multiple replicate intracranial patient-derived xenografts(PDX) revealed that recurrent tumors were characterized by a gene expression pattern characteristic of a mesenchymal and CSC signature, which include upregulation of *THY1/CD90, TGFβ1, TGFβ2, SOX2, ZEB2, and GLI2*. Consistent with previous observations, we demonstrate using a large GBM cohort that this gene expression profile is associated with a worse overall prognosis, highlighting the clinical implications of our findings. To test the hypothesis that tumor recurrence may be attributed to a pre-existing cell population characterized by this gene expression signature, we immunosorted THY1+ cells from treatment-naïve patient samples and demonstrated that intracranial tumors derived from THY1+ cells (Pre-THY1+) were inherently treatment resistant compared to unsorted tumors. These results suggest that rare populations of inherently treatment-resistant, recurrence initiating cells with distinct gene expression profiles can be found within the original treatment-naïve tumors, and may be responsible for tumor recurrence [5,8,12]. In support, treatment of tumors with a targeted agent that reverses the mesenchymal gene expression signature, resulted in restoration of sensitivity to chemoradiation. Furthermore, spatial transcriptomic analyses of human GBM specimens consistently identified *THY1+* cells co-localized with expression of mesenchymal, glioma stem cell, and macrophage gene signatures and were primarily found within a perivascular niche. This suggests an important role for these rare resistant cells in the vascular tumor microenvironment.

## Materials and methods

### *Patient-derived primary neurosphere culture*

Low passage, patient-derived primary GBM neurosphere cells, HF2303, have been previously described [13,14], and were maintained in neurosphere medium composed of DMEM/F12 medium (#11320-033, Life Technologies, Carlsbad, CA) plus N2 supplement(#17502-048, Life Technologies, Carlsbad, CA), 0.5mg/ml BSA (#A4919, Sigma-Aldrich Co., St. Louis, MO), 25μg/ml Gentamicin (#15750-060, Life Technologies, Carlsbad, CA), 0.5% antibiotic/antimycotic (#15240-096, Life Technologies, Carlsbad, CA), 20ng/ml bFGF and 20 ng/ml EGF (#100-15 and #100-18B, PeproTech, Rocky Hill NJ). These cultures were derived from resected brain tumor specimens collected at Henry Ford Hospital (Detroit, MI) with written informed consent from patients, under a protocol approved by the Institutional Review Board. This patient-derived line represented a mesenchymal subtype IDH-wildtype GBM that is MGMT unmethylated with p53 mutation, PTEN loss, and associated gain of chromosome 7 and loss of chromosome 10. This original cell line and subsequent lines derived from animal models were analyzed with RNA sequencing to assess for gene expression changes.

### *Stereotactic biopsy*

All research involving animals complied with protocols approved by the University Committee on Use and Care of Animals (Protocol # PRO00008583). Coordinates for MRI-guided biopsy were determined by a fiducial markers attached to the whole-body volume transmit coil and VnmrJ software (Agilent Technologies, Inc., Santa Clara, CA) [15] (Fig. S1). The mouse was moved to a stereotactic station along with the whole-body volume transmit coil. A 1cm incision was made and the skull was exposed with cotton-tip applicators. After biopsy location was recovered using the fiducial markers, a burr hole was drilled and a 22GA x 3 7/8″ needle (#54722, Inrad, Kentwood, MI) attached to a vacuum syringe was inserted into the tumor. Biopsy tissues were dissociated and cultured in NMGF medium immediately and were expanded for three passages, to eliminate non-dividing cells derived from normal mouse brain. Holes were covered using bonewax and incisions were sealed using Vetbond. 100ul of carprofen was subcutaneously injected following the surgical procedure.

### *Treatment*

For mice bearing intracranial tumors, animals were randomized into treatment groups once their tumor volume reached 20-30mm$^3$ by MRI evaluation (Fig. 1). Temozolomide (LKT Laboratories, St Paul, MN) was suspended in Ora-Plus suspending vehicle (#0574-0303-16, Rotterdam, Netherlands) and administered to animals (66mg/kg) via oral gavage daily for five days per week. Cranial irradiation was carried out one hour post temozolomide treatment. Mice were restrained in a home-made plastic restraining device. A lead shield was used so that only the head was exposed to radiation using a Kimtron INC-320 orthovoltage irradiator (Kimtron Medical, Oxford, CT). A total of 20Gy radiation was delivered to each animal at 2 Gy/day for ten days. Maintenance temozolomide was delivered orally three times week every other week from the third week till animals became moribund. For mice with subcutaneous flank tumors, animals were randomized into study groups when subcutaneous tumors reached an approximate volume of 300 mm$^3$. Temozolomide and radiation were delivered via similar administration routes and treatment schedules as described above. Radiation was targeted at local tumor sites with a lead shield. LY2109761(50mg/kg) (AbMole, Houston, TX), a TGF$\beta$RI inhibitor, was reconstituted using Ora-Plus suspending vehicle and delivered to animals twice per day for five days every week for two weeks. For animals treated with temozolomide, LY2109761 and radiation, LY2109761 was administered one hour before radiation along with TMZ and six hours after radiation treatment.

### *Cell line transfection, proliferation and TMZ/IR sensitivity*

U87 and D54 cells were obtained from ATCC. SF268 cells were obtained from NIH-Division of Cancer Treatment and Diagnosis (DCTD) Repository. For THY1 overexpression, clone THY1_OHu08788C (Genscript) was cloned into pGenlenti vector and transfected in U87 cells. Cells were selected using 1ug/ml puromycin and grown as neurospheres prior to performing assays. For knockdown studies, Sigma shRNA constructs THY1#1: clone ID TRCN0000057024 and shRNA#2: THY1_E12: clone ID TRCN0000057027were used to target THY1. D54 and SF268 cells were maintained in adherent cell culture format using DMEM with 10% serum. U87 cells were grown as neurospheres in low attachment plates (Nunclon) in serum free media with bFGF and EGF obtained from, PeproTech, Rocky Hill NJ at 20 ng/ml each. Cells were selected with puromycin 1ug/ml for at least three days. For cell proliferation assays, 2000 cells were plated/well in 96-well plates and CellTiter-Glo (Promega) was utilized to assess cell counts after 7 days. U87 neurospheres were treated with varying concentrations of TMZ and were

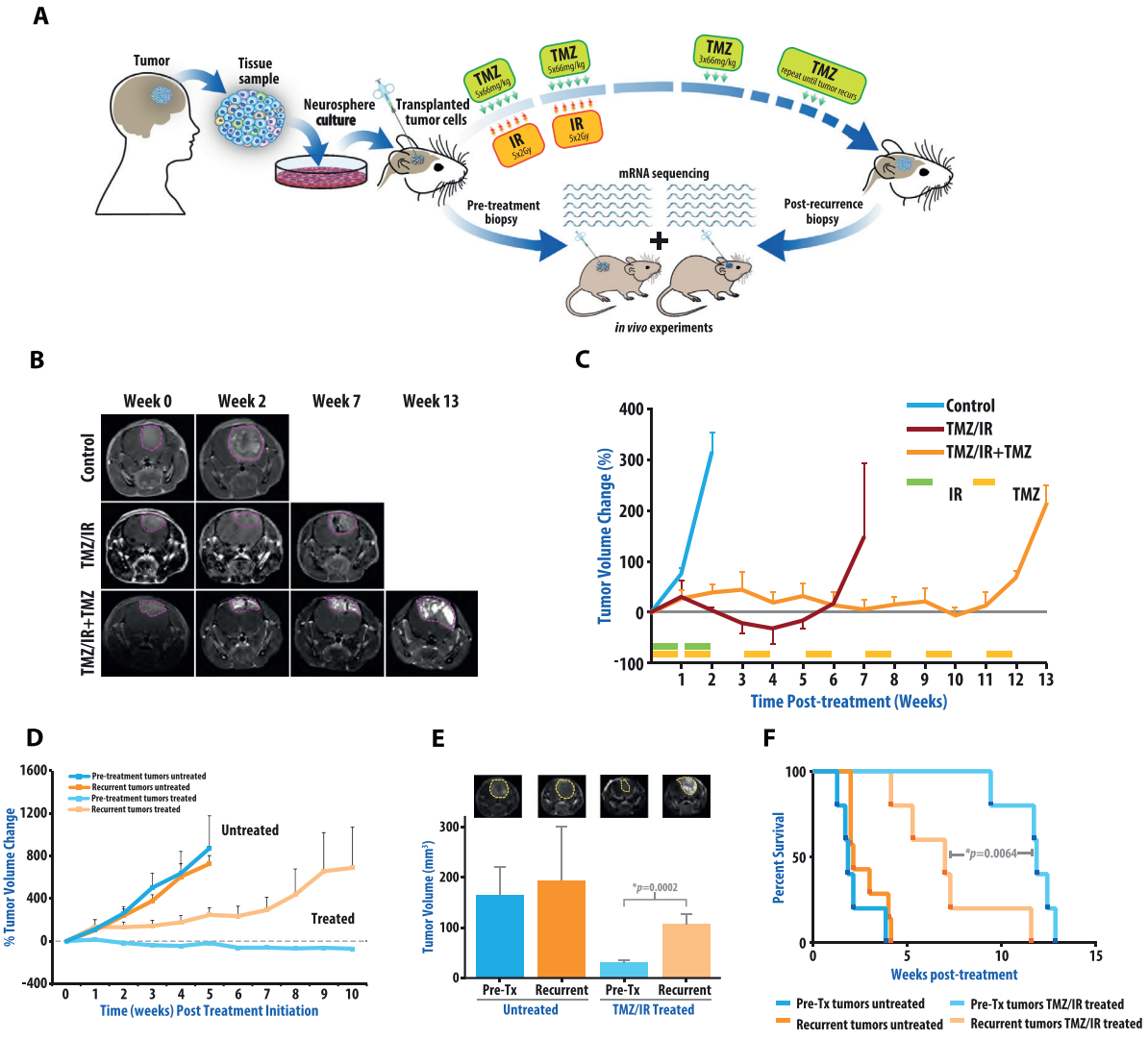


**Fig. 1.** Analysis of longitudinal intracranial GBM samples, pre-treatment and at recurrence, reveals development of a therapeutic resistant phenotype. (A) Schematic of experimental design. Mice bearing intracranial tumors derived from human GBM explants are treated with concomitant temozolomide (TMZ) and radiation (IR) for two weeks followed by adjuvant TMZ until animals became moribund. Tumor biopsies are obtained pre-treatment and at recurrence to provide samples for molecular analysis and additional *in vivo* and *in vitro* comparative studies. (B) Representative MR images from Control, TMZ/IR and TMZ/IR+TMZ treatment groups at 0, 2, 7 and 13 weeks post-initiation. (C) Treatment response quantified using MR-imaging derived tumor volume changes in Control, TMZ/IR and TMZ/IR+TMZ intracranial tumor bearing groups. TMZ/IR treatment involved 2 weeks of concomitant TMZ/IR, while mice receiving TMZ/IR+TMZ received the initial 2 week treatment followed by maintenance adjuvant TMZ every other week. Percent change in tumor volume is shown as mean change in a cohort of five animals with SEM. (D) Pre-treatment(Pre-Tx) and post-treatment(recurrent) biopsy samples were re-implanted subcutaneously into the flanks of mice to evaluate their sensitivity to treatment as described in methods(Median volume +SEM shown). Pre-treatment and recurrent tumors show similar growth rates in the absence of treatment, while recurrent tumors exhibit an inherent resistance to TMZ/IR. (E) Samples described in D were also evaluated intracranially. Tumor volumes derived from pre-treatment and recurrent tumors with or without TMZ/IR are shown as mean tumor volumes (+SEM) as well as representative MR images three weeks after treatment initiation. (F) Kaplan-Meier survival curve of mice after intracranial implantation of pre-treatment and recurrent tumors with or without TMZ/IR treatment. Mice bearing recurrent tumors have significantly worse survival with treatment. Animal experiments were performed with 5 replicates.

tested to assess dose response and establish $IC_{50}$ values. These cells were also treated with a single fraction of 2Gy of ionizing radiation on the second day of the experiments. Cell counts were determined utilizing CellTiter-Glo after 7 days. All experiments were performed at least as duplicates.

*Generation of UM3506 organoids and related assays*

Patient derived tissue was processed as previously described [16]. Briefly, freshly resected GBM tissue was cut into 0.5-1mm pieces and placed in GBO medium containing 50% DMEM:F12 (Thermo Fisher Scientific), 50%Neurobasal (Thermo Fisher Scientific), 1X GlutaMax (Thermo Fisher Scientific), 1X NEAAs (Thermo Fisher Scientific), 1X PenStrep(Thermo Fisher Scientific), 1X N2 supplement (Thermo Fisher Scientific), 1X B27 w/o vitamin A supplement (Thermo Fisher Scientific),1×2-mercaptoethanol (Thermo Fisher Scientific), and 2.5 mg/ml human insulin (Sigma) per well and placed on an orbital shaker rotating at 120 rpm within a 37_C, 5% CO2, and 90% humidity sterile incubator. Organoids were maintained by refreshing 75% of the media every three days with fresh GBO medium. 50-60 organoids were then transfected with the indicated shRNA or sgRNA constructs and selected using 1ug/ml of puromycin. shRNA sequences are as detailed earlier. sgTHY1 (sequence:ACAAAGAAGCACGTGCTCTT) was cloned into pLentiCRISPRv2 eSpCas9 (GenScript) for the inducible knockout studies. To test oncogenicity of organoids, 20 organoids (corresponding to 75,000 cells in suspension) were injected intracranially in mouse brains as de-

scribed earlier. For TMZ sensitivity assays 200 organoids were separated into two 24 well culture dishes and 1ug/ml doxycycline was added to one set of organoids. After two days the treated and untreated organoids were collected by centrifugation and replated onto 96 well plates (30 organoids each) and cultured in the presence or absence of varying concentrations of TMZ. Cell counts were determined utilizing the 3D CellTiter-Glo reagent and luminescence measurements were recorded. All experiments were performed at least as duplicates. Patient tumor sample genetic analyses performed utilizing commercial Tempus 648 gene panel (Tempus, Chicago, IL). All data analysis was performed using GraphPad Prism, version 9.1.0.

*Spatial transcriptomics*

Under an institutional review board approved study in accordance with recognized ethical guidelines, intraoperative brain tumor specimens were collected at the University of Michigan using MRI-imaged guidance technology to localize specimen within contrast-enhanced tissue with low and high perfusion parameters. We utilized contrast enhanced T1-weighted MRI and perfusion MRI parameters to identify sites of interest. For perfusion studies, we utilized the relative cerebral blood volume parameter derived from dynamic susceptibility contrast MR perfusion. Two accessible sites with contrast enhancement with the highest and lowest perfusion were identified and determined for intraoperative biopsy. The image sets are loaded and co-registered onto our stereotactic navigation system (Stryker, Kalamzoo, MI) and these sites are identified after exposure with our stereotactic localization device, and biopsies are performed prior to resection of the tumor. This research was in full compliance of all pertinent ethical regulations for research with human biospecimens and all data were de-identified (IRB HUM00175135). Human samples acquired were immediately frozen in liquid nitrogen/isopentane, after which they were imbedded in optimal cutting temperature compound and frozen. Tissue was sectioned onto Visium Spatial Gene Expression Slide(10X Genomics) and permeabilized to release mRNA to bind to spatially barcoded capture probes. Further details of the sequencing and analysis are provided in the supplementary materials.

*Statistics*

Results of *in vivo* volume data are shown as mean with standard error with 5 replicates performed for studies. Student's t-test (unpaired) and ANOVA was performed to assess statistical significance with $p<0.05$ considered significant. Survival analyses were performed utilizing Kaplan-Meier survival and statistical significance tested utilizing log-rank (Mantel-Cox) analyses with p-values as shown utilizing Graphpad Prism(9.0). Publicly accessible data from The Cancer Genome Atlas(TCGA/Firehose Legacy dataset) and Glass Consortium [17] were analyzed for gene sets of interest.

*Data availability statement*

The data generated in this study are publicly available in the Sequencing Read Archive (SRA) at PRJNA826117.

## Results

In vivo *modeling recapitulates therapeutic response to TMZ/IR followed by recurrence*

To evaluate the therapeutic response and the underlying genetic basis for resistance to standard of care therapy (TMZ/IR) in GBM, we utilized patient-derived explants in intracranial xenografts (Fig. 1). Magnetic resonance imaging was performed weekly to monitor tumor growth after implantation. Mice bearing tumors of approximately $20mm^3$ were randomized into three study cohorts. The first represented control untreated animals, and a second cohort was treated with concurrent TMZ/IR for two weeks. A third cohort was administered concurrent TMZ/IR for 2 weeks followed by adjuvant TMZ three times a week, every other week after completion of the second week of TMZ/IR. This experimental design was intended to investigate mechanisms of resistance to standard of care therapy (Fig. 1A). In contrast to control animals which exhibited a greater than 300% increase in tumor volume and succumbed to disease by the third week, TMZ/IR treated animals exhibited an initial tumor regression and survived beyond six weeks. Mice that received adjuvant TMZ exhibited a greater delay in tumor growth and had a prolonged survival (>12 weeks). Despite an initial response to therapy, all treated animals had recurrence (Fig. 1B and 1C).

To better understand the underlying genetic basis for the development of therapeutic resistance, an MRI-guided stereotactic intracranial biopsy was used to obtain tumor tissue from animals prior to initiation of treatment. This biopsy procedure does not significantly impact the gross tumor architecture [15] (Fig. S1). Viable tumor tissue was also obtained from these animals upon recurrence. The paired pre-treatment and recurrent tumor samples were collected for further analyses.

*Recurrent tumors are distinctly resistant to TMZ/IR*

To evaluate the sensitivity of recurrent tumors to therapy, paired neurosphere cultures derived from pre-treatment and recurrent biopsies were implanted intracranially and subcutaneously into immune-deficient mice. Subcutaneously implanted murine models with palpable tumors were randomized into a control group or treated with TMZ/IR for two weeks followed by adjuvant TMZ as above. In the absence of treatment, both the pre-treatment and recurrent tumors obtained by biopsies grew at a similar rate. In response to TMZ/IR, pre-treatment tumors demonstrated a significant delay in tumor growth (analogous to the initial patient-derived tumors), and exhibited a 50% decrease in tumor volume. However, tumors derived from recurrent biopsies continued to exhibit resistance to TMZ/IR, and demonstrated a 750% increase in tumor volume (Fig. 1D). To confirm these findings in an appropriate tumor microenvironment, intracranial tumors were established using the same paired neurospheres. Treatment of mice bearing intracranial recurrent tumors with TMZ/IR plus adjuvant TMZ demonstrated their resistance to therapy compared to those derived from pre-treatment samples (Fig. 1E). In support, the median survival of mice bearing recurrent tumors was 7 weeks compared to 11.9 weeks for treatment naïve tumors ($p=0.006$) (Fig. 1F).

*Recurrent tumors develop a therapeutic resistant phenotype with increased mesenchymal and stem cell gene expression patterns and* THY1 *upregulation*

To delineate the underlying basis for the observed resistance to therapy in recurrent samples, transcriptomic analysis of at least three independent replicates of pre-treatment and recurrent biopsies from the same subject animals was performed using RNAseq (Fig. 2A). 1159 genes were found to be differentially expressed (FDR<0.05). Among these differentially expressed genes, 645 genes were upregulated in recurrent tumor samples while 514 genes were downregulated. Unsupervised clustering analysis showed distinct transcriptomic profiles of the pretreated and recurrent tumors across multiple replicates (Figs. 2B, S2). Moreover, the transcriptome of each pre-treatment sample closely resembled that of the original patient derived neurosphere cultures, demonstrating that the gene expression profile did not drift significantly after *in vitro* expansion or upon intracranial implantation.

Next, we carried out a Gene Ontology analysis using Database for Annotation, Visualization and Integrated Discovery (DAVID) to identify cellular processes enriched in tumors with TMZ/IR resistance. Recurrent tumors showed altered biological processes as 20 upregulated and 13 downregulated functional clusters (FDR<0.05). These clusters were further consolidated to yield a non-redundant set of 10 upregulated gene clusters and seven downregulated gene clusters (Fig. 2C).

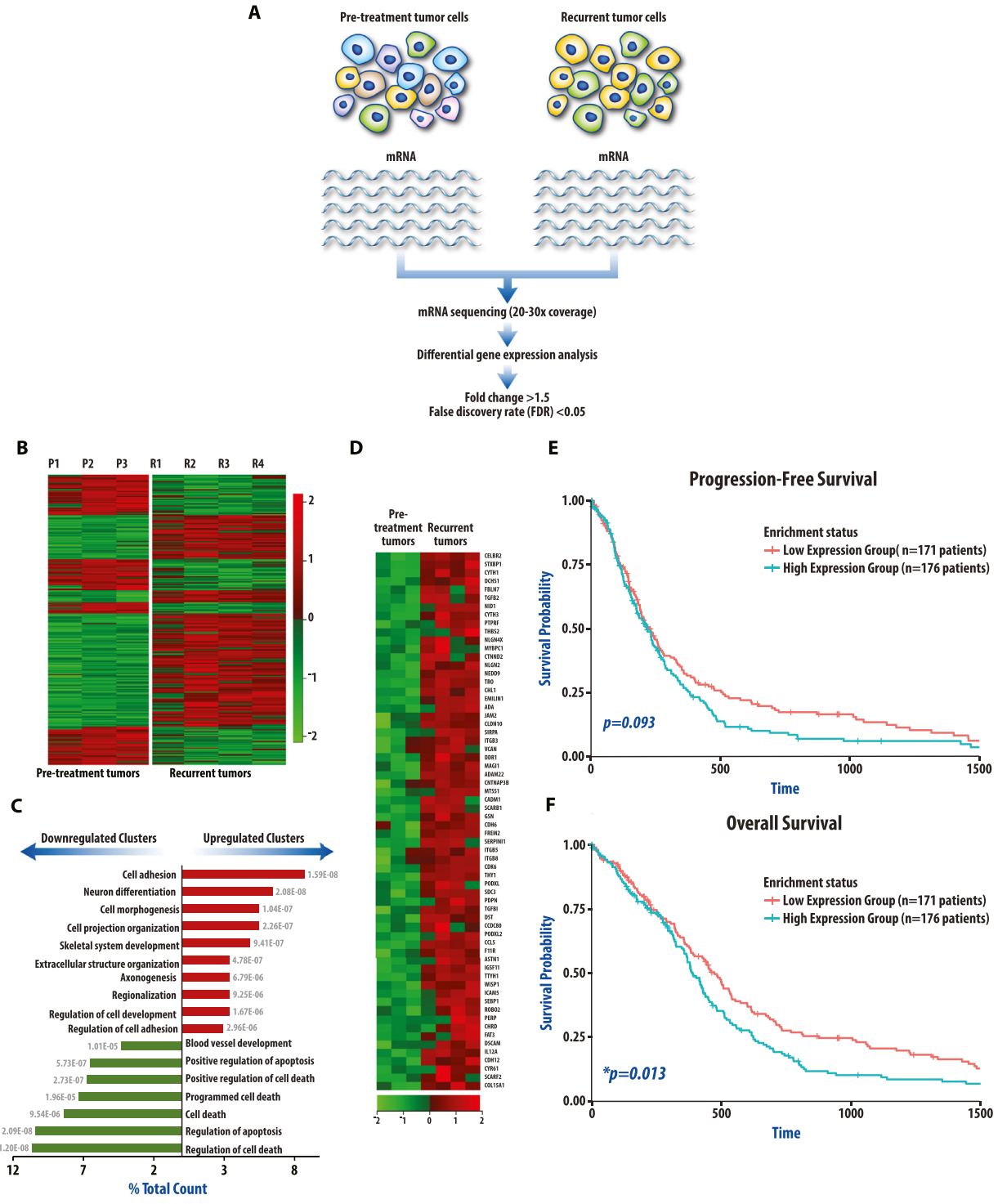


**Fig. 2.** RNAseq analyses reveal a resistant gene expression profile that predicts outcomes in clinical datasets. (A) A diagrammatic representation of the experimental workflow. Paired pre-treatment and recurrent tumor samples are evaluated by next generation sequencing of RNA samples extracted from cells. (B) Unsupervised clustering analysis revealed that replicate independent pre-treatment samples clustered together had a similar gene expression pattern. Similarly independent replicate recurrent samples clustered together. Heatmap of differentially expressed genes in independent pre-treatment biopsies (P1,P2,P3) and recurrent tumor biopsies (R1,R2,R3,R4). (C) Functional clusters of upregulated and downregulated genes in recurrent tumors. Bar graph shows percentage of gene counts of each cluster compared to total upregulated or downregulated genes. P-value of each cluster is labeled next to each bar. Cell adhesion genes were upregulated in recurrent tumors. (D) Heatmap of individual genes within the highest upregulated clusters. Overall (E) and progress-free survival (F) of GBM patients with high and low expression levels of a signature characterized by cell adhesion genes, showing that this upregulated signature predicts outcomes in GBM patients(TCGA, Firehose Legacy microarray data).

Of the seven downregulated clusters, six were associated with apoptosis and cell death. Genes involved in cell adhesion, neuronal differentiation/development, and cellular morphogenesis were dominant in the upregulated clusters. Particularly, recurrent tumors overexpressed genes related to cell adhesion (Fig. 2D) (e.g. *ITGB3, ITGB5, ITGB8, NEDD9, FBLN7, NLGN2, CADM1 and VCAN*) and those associated with a mesenchymal phenotype (*TGFB2, TGFB1, THY1*). In fact, within the most upregulated cluster, 21 of the 64 genes (Fig. 2D) were associated either directly or indirectly with the TGF$\beta$ pathway.

Upregulation of this gene expression signature was found to be associated with a therapy resistant phenotype as indicated by a worse prognosis in the TCGA. A metagene score was created based on the average gene expression level of the top 64 cell adhesion genes. As shown in Fig. 2F, patients with a high metagene score had worse overall survival (p=0.013). This analysis corroborates our observations from the experimental mouse model that an increase in the experimentally observed signature correlates with therapeutic resistance in patients.

To explore the role of genes associated with cell adhesion, mesenchymal and stem cell phenotype in TMZ/IR resistance, we first validated select genes from RNAseq analysis (*ZEB2, VCAN, CDK6, THY1, GLI2, SOX2*) which have previously been associated with therapeutic resistance in GBM [18–21]. Quantitative PCR analysis confirmed that *ZEB2, VCAN, CDK6, THY1, GLI2,* and *SOX2* mRNA levels were upregulated in all four recurrent tumor samples compared to their treatment naïve counterparts (Fig. 3A,B). Western blot analysis confirmed that the protein levels for each of these genes were also increased in a majority of recurrent samples compared to their untreated counterparts (Fig. 3C,D). Expression of the CD133 cell surface epitope, a marker of glioma stemness, was also markedly elevated in three of the four recurrent tumors (Fig. 3B).

In contrast to these consistent changes in gene expression observed between replicate recurrent tumors, analysis of copy number gain or copy number loss between each of the pre-treatment and recurrent samples did not show any significant and consistent changes (Fig. S3). This suggests that development of the resistance phenotype resulted from changes in gene expression rather than genomic changes, highlighting the importance of modulation of the relevant cell signaling pathways identified.

The patient from which this PDX line was derived also had a post-treatment recurrence that was resected and available for comparative analysis from the TCGA(TCGA 06-0190). Hallmark pathway enrichment analysis of the matched pre-treatment and recurrent specimens revealed epithelial to mesenchymal transition as the most significantly upregulated pathway at recurrence ($p=2.7\times10^{-9}$). We then performed an Ingenuity Pathway Analysis [22] and found that the TGF$\beta$ pathway, a known master regulator of epithelial to mesenchymal transition was the most significant upstream regulator of gene expression changes at recurrence ($p=2.0\times10^{-46}$, z-score 2.87). Evaluation of specific mesenchymal pathway genes in this patient also revealed upregulation of genes previously identified in our recurrence mouse modelling studies, including TGF$\beta$1, THY1, VCAN, TGF$\beta$2, GLI2, and ZEB2 (Fig. 3E).

### *Inhibition of TGFβ signaling decreases* THY1 *expression, reverses the mesenchymal resistance phenotype, and results in improved treatment sensitivity* in vivo

Since the pre-clinical and clinical results directly implicated the TGF$\beta$ signaling pathway with recurrence, we evaluated the significance of this association using an inhibitor of the TGF$\beta$R1 serine threonine kinase. Animals bearing flank tumors derived from pre-treatment (P2) as well as recurrent tumors (R1) were randomized into four groups: 1) Control (untreated), 2) TMZ/IR treatment, 3) Treatment with TGF$\beta$ inhibitor alone (LY2109761), and 4) treatment with a combination of TMZ/IR and LY2109761. Western blot analysis of untreated tumor samples (P2 and R1) as well as treated recurrent tumor samples (RT1-5) revealed that treatment of tumors with LY2109761 resulted in decreased levels of THY1, ZEB2, CDK6, SOX2, and GLI2 compared to the untreated recurrent tumors (Fig. 3F). Furthermore, these markers of a mesenchymal/stem phenotype were also downregulated in tumors that received TMZ/IR and concurrent LY2109761. These findings demonstrate that LY2109761 appropriately targeted the pathways of interest as expected in our models of GBM.

Single agent treatment with LY2109761 did not significantly slow tumor growth (Fig. 3G). However, combining LY2109761 with TMZ/IR substantially decreased tumor growth compared to TMZ/IR treatment alone (mean volume 117cc vs 235cc, respectively, p=0.2). Although the difference was not significant suggesting that the combination may not be synergistic, there was a clear additive effect. In combination with our protein expression analysis and the upstream pathway analysis of the patient matched samples, these findings suggest that TGF$\beta$-mediated activation of mesenchymal and stem-like gene expression profiles promotes resistance to TMZ/IR, and that TGF$\beta$ inhibition downregulates the mesenchymal and stem-like phenotype restoring sensitivity to TMZ/IR.

### *Rare THY1+ cell populations derived from treatment naive GBM are inherently TMZ/IR resistant, and repopulate the recurrent tumors*

The above finding that *THY1* transcript and protein levels were upregulated within the recurrent tumor samples (more than 100-fold compared to treatment-naïve samples, Fig. 3A), combined with the observation that LY2109761 treatment resulted in decreased *THY1* expression and restored the sensitivity of recurrent tumors to TMZ/IR (Fig. 3F and 3G respectively), prompted us to investigate *THY1* further. In human cancers, *THY1* is associated with a poor prognosis, is linked with cancer stem cells and plays a role in cell signaling, adhesion, invasion, metastasis, immune evasion, and epithelial to mesenchymal transition [21,23,24]. Given the association of *THY1* expression with treatment resistance and a mesenchymal signature, its notable upregulation within the recurrent tumor samples, and its status as a cell surface marker, we quantitatively evaluated the presence of THY1+ cells in our tumors. In the treatment-naïve tumor biopsies we observed that THY1+ cells constituted 6-10% of the population. In contrast, 75-96% of the cells within recurrent tumors were THY1+ (Fig. 4A,B). FACS isolation and expansion of THY1+ cells from pre-treatment samples (Pre-THY1+), confirmed that they retained the expression of cell surface THY1 (Fig. 4C,D). Pre-THY1+ cells were then implanted intracranially into nude mice and treated with TMZ/IR. These experiments revealed that the Pre-THY1+ cells were in fact inherently treatment resistant to a degree that mirrored the recurrent tumors (Fig. 4E). Additionally, the survival of mice bearing intracranial tumors derived using Pre-THY1+ cells was similar to mice with tumors derived from recurrent cells (p=0.6) (Fig. 4F), and was notably worse than mice with pre-treatment tumors (median survival of 61 vs 82 days, respectively, p=0.06). This finding, combined with the consistent observation that each of the recurrent tumors (R1-R4, Fig. 4A) exhibited an enrichment of THY1+ cells when compared to their respective pre-treatment biopsy (P1-P3, Fig. 4A) suggests that THY1+ cells represented a treatment recalcitrant cell population within the treatment-naïve tumors. These cells have a mesenchymal phenotype, and likely survive therapeutic intervention and repopulate the tumor.

To assess the clinical significance of upregulated *THY1* and its association with treatment resistance, we interrogated RNAseq data from 31 orthotopic GBM PDX models treated with standard therapies (TMZ, IR, or TMZ/IR) published in a recent study [25]. This analysis revealed that THY1, one of the most highly expressed genes in our recurrent samples, was associated with TMZ/IR resistance with a magnitude of correlation similar to MGMT, the most clinically useful biomarker of treatment resistance (Fig. 4G). These results further corroborated the findings of our initial PDX model. We then analyzed the TCGA database which showed that high *THY1* expression was associated with significantly worse overall survival (p=0.012) (Fig. 4H). We also analyzed paired human GBM specimens from the GLASS consortium [17] and other clinical databases [26–28] which revealed that *THY1* gene expression is significantly up-

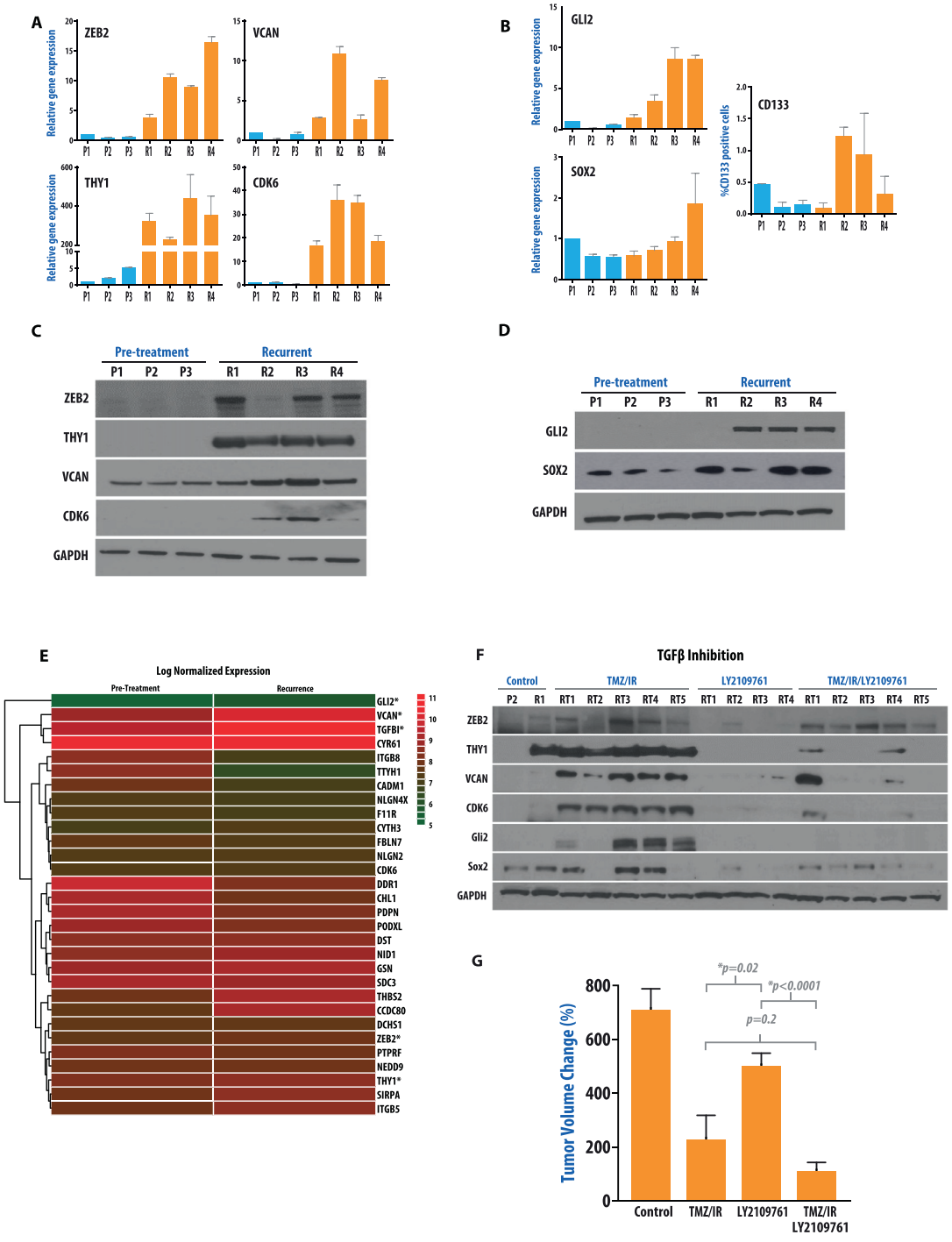


**Fig. 3.** Analyses of paired samples reveals development of a therapeutic resistant phenotype with a mesenchymal gene expression pattern that is reversed with TGF$\beta$ inhibition. (A) Upregulated genes in recurrent samples (R1-R4) associated with a mesenchymal signature were confirmed by qRTPCR, show notable upregulation in recurrent samples compared to pre-treatment samples (P1-P3). THY1 is most prominently differentially upregulated, greater than 100-fold compared to pre-treatment levels. Analyses performed in triplicate. (B) Upregulated genes in recurrent samples associated with a stem cell phenotype were confirmed using qRTPCR. FACS analysis of CD133 expression in pre-treatment and recurrent neurosphere cells (bottom right panel) shows upregulation of CD133+ cells in 3 of 4 samples at recurrence. qRTPCR Analyses performed in triplicate with standard error bars shown. (C, D) Western blot analysis confirmed that the protein levels for each of these genes were also increased in the majority of recurrent samples compared to their untreated counterparts. (E) Analysis of paired clinical specimens (pre-treatment and recurrent) from the patient from which the PDX line was derived was performed (TCGA 06-0190) and showed upregulation at recurrence of many of the genes identified in the recurrent mouse model (* indicating genes of interest). (F) Western blot analysis shows that inhibition of TGF$\beta$ signaling results in a marked decrease in expression of proteins associated with a mesenchymal and stem cell signature in recurrent tumor samples. P2 (treatment naïve sample 2). R1 (recurrent sample 1), RT1-RT5 (recurrent samples treated as indicated in five independent animals) with TMZ/IR, LY2109761, or combination of TMZ/IR and LY2109761 as described below. (G) Animals bearing flank pre-treatment tumors as well as recurrent tumors were randomized into four groups: 1) An untreated group (control), 2) Treatment with TMZ (TMZ, 5 days/week at 66mg/kg) and IR (5 days/ week at 2Gy) for two weeks followed by TMZ (3 days/week at 66mg/kg) every other week (TMZ/IR), 3) Treatment with LY2109761 where mice received 50mg/kg LY2109761 twice every day, 5 days/week for the first two weeks followed by 3 days/week every other week (LY2109761), and 4) TMZ/IR/LY2109761 group where the animals were treated with a combination of the three aforementioned treatment modalities. 5 animal replicates were evaluated. Mean volume + SEM shown. p-values shown with *signifying p<0.05.

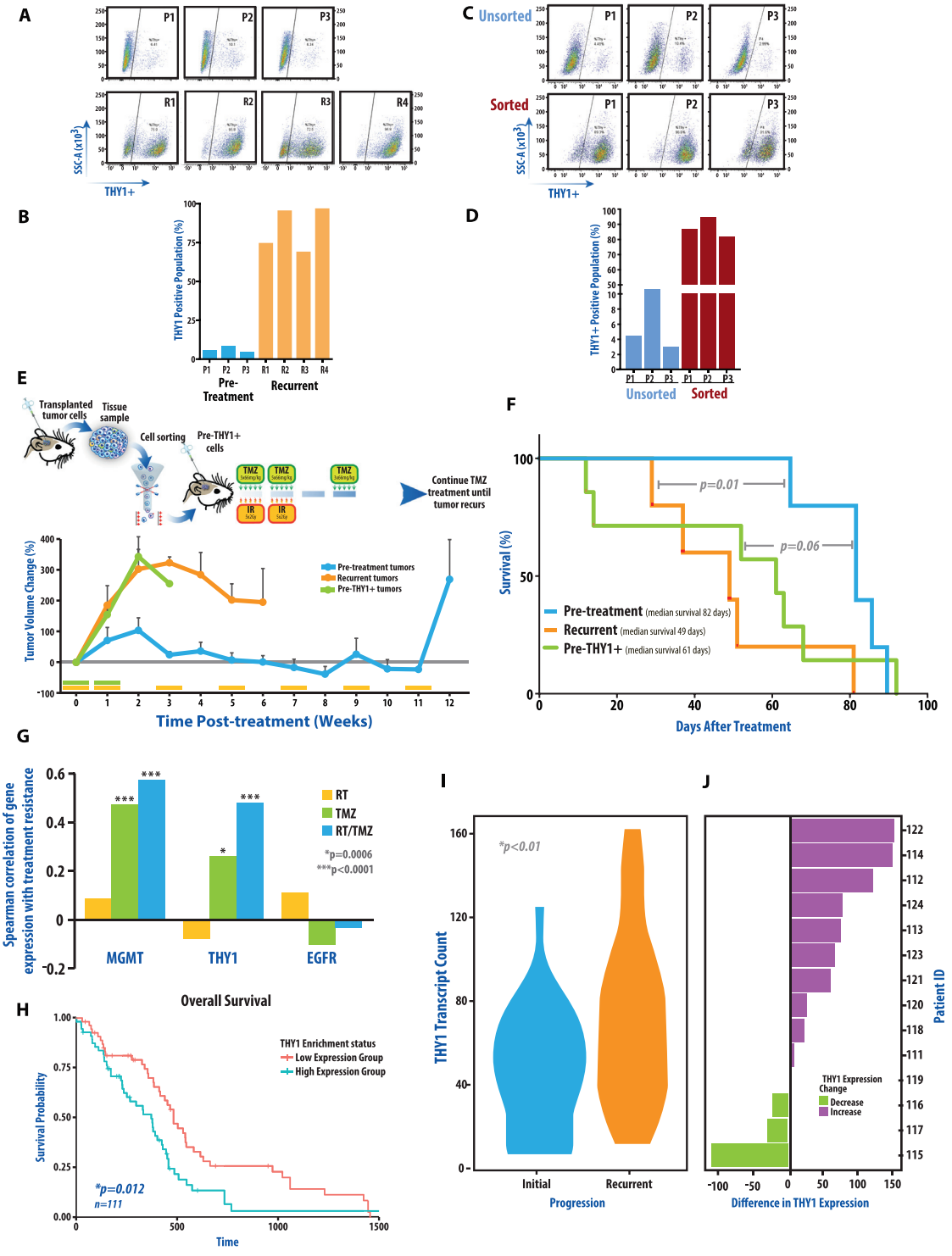


**Fig. 4.** Rare THY1+ cell populations are identified in the pre-treatment samples, are inherently treatment resistant, and repopulate the recurrent tumors. (A) THY1 cell positivity is highly upregulated in recurrent samples as seen by flow cytometry and representative bar graph (B). 6-10% of pre-treatment samples (P1-P3) demonstrate THY1-positivity while 72-96% of recurrent samples (R1-R4) reveal THY1-positivity(left) with quantification of replicate experiments shown(right). (C, D) THY1-positive cells were immuno-purified from P1, P2 and P3 samples by FACS. This sorted THY1+ cell population was cultured for expansion and re-tested to confirm stable THY1 cell surface staining. (E) Sorted THY1+ cell population from P2 (Pre-THY1+) was implanted intracranially to assess treatment response. Resistance to TMZ/IR was observed in the Pre-THY1+ tumor bearing animals that mirrored the phenotype observed in recurrent tumors, but distinct from pre-treatment samples. Mean tumor volume (E) (+SEM) and survival analysis by Kaplan-Meier (F) are shown. 5 animal replicates were evaluated. (G) RNAseq analysis of 31 orthotopic GBM PDXs treated with standard therapies were used to determine Spearmans correlation value as described in the text [96]. Bar chart showing association of the indicated gene expression with treatment resistance. This analysis revealed that THY1, one of the most highly expressed genes in our recurrent samples, was associated with TMZ/IR resistance with a magnitude of correlation similar to MGMT. EGFR was used as a negative control. *indicates p-value=0.0006 and FDR=0.04 and ***indicates p-value<0.00001 and FDR below 0.0007. (H) Evaluation of RNAseq data from the TCGA (TCGA, Firehose Legacy) reveals THY1 expression is associated with significantly worse overall survival. (I) Analysis of longitudinal GBM specimens reveals significant upregulation of THY1 expression in recurrent tumors(GLASS consortium) with most patients showing increased expression (J).

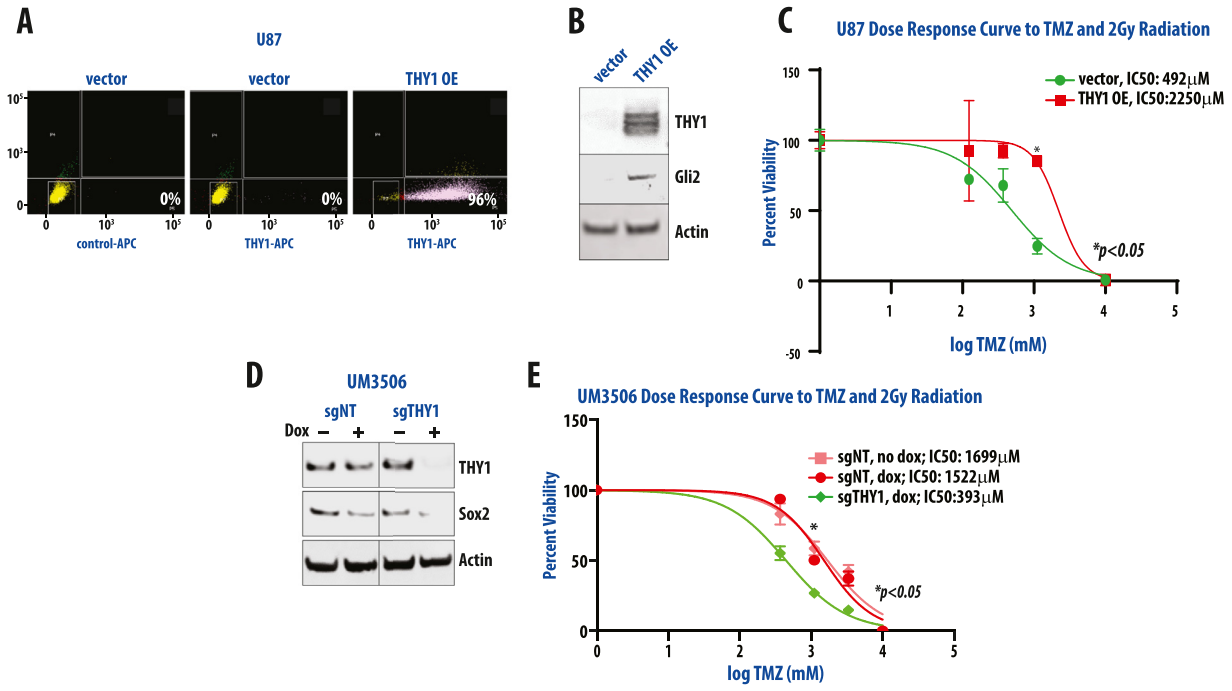


**Fig. 5.** Induction of THY1 overexpression results in increased treatment resistance, whereas THY1 doxycycline-inducible knockout results in increased treatment sensitivity. U87 high grade glioma lines with baseline low THY1 expression were induced to overexpress THY1. (A) Flow cytometric analysis of U87 cells expressing either an empty vector or THY1 overexpression (THY1 OE). APC-conjugated control IgG is used as control. Percentages indicate THY1 membrane expression in indicated cells (B) Western blot analysis of U87 cells over-expressing THY1. Data shown represents analysis of indicated proteins separated on the same gel. (C) TMZ/IR dose response curves of U87 cells expressing either vector or THY1 OE with $IC_{50}$ values shown. * indicates p-value of 0.05 using paired t-test analysis. (D) Western blots of lysates were obtained from the UM3506 organoid lines after 3 days of doxycycline treatment. Data shown represents analysis of indicated proteins on the same gel. (E) TMZ dose response curves of doxycycline-induced control sgRNA and sgRNA targeting THY1 in UM3506 organoid lines after 7 days. $IC_{50}$ values shows. * indicates p-value<0.05 obtained after paired t-test to compare dose response curves with doxycycline treated non targeting sgNT line. Experiments were performed in duplicates and repeated at least two times. OE= Overexpression; NT = non-targeting.

regulated at recurrence (Figs. 4I,J; S4). Utilizing single cell RNA sequencing, we then interrogated 2 treatment-naïve and 2 recurrent patient GBM biopsies and identified that the proportion of THY1+ cells is notably increased in recurrent tumors, and that *THY1* expression is significantly upregulated within tumor cells at recurrence (Fig. S4D,E). These findings illustrate that our model paralleled the clinical scenario, and further emphasize the role of *THY1* in the development of TMZ/IR resistance, and suggests that clonal expansion of THY1-expressing GBM cells likely contributes towards TMZ/IR resistance.

We then functionally assessed the role of THY1 in treatment resistance by overexpressing THY1 in U87 high grade glioma cells that have low endogenous levels of THY1 (Fig. 5). When treated with increasing concentrations of TMZ with 2Gy of radiation we observed a significant increase in the $IC_{50}$ levels (4.6-fold) in THY1 overexpressing U87 cells ($p<0.05$) (Fig. 5C) compared to vector control U87 cells. We then induced small hairpin RNA (shRNA) mediated THY1 knockdown in two high grade glioma cell lines which had high THY1 expression at baseline. In both D54 (Figs. S5A) and SF268 (Fig. S5B) cells, THY1 knockdown resulted in significantly decreased cell proliferation.

To further explore the role of THY1 in a more clinically relevant patient-derived tissue, we generated patient-derived organoids from freshly resected IDH wildtype GBM specimens obtained from the operating room. This freshly isolated tissue (UM3506) had a mesenchymal gene expression profile (NF1 mutation, PTEN mutation, as determined by the Tempus panel) and high baseline THY1 expression (Fig. S5D). These organoids were engineered to conditionally express shRNAs targeting THY1(Fig. S5E). Similar to the cell line models described above, reduced THY1 levels led to significant reduction in proliferation of the organoid cultures (Fig. S5F). To confirm that the observed phenotype was not due to off target effects of the shRNA, we used a doxycycline-inducible Tet-On CRISPR/Cas9 system to knock out the THY1 locus in high THY1 expressing UM3506 cells. Dose response curves showed reduced sensitivity to TMZ/IR upon THY1 knockout (Fig. 5F) ($p<0.05$). $IC_{50}$ values were 4.8-fold lower in THY1 knockout organoids when compared to control. In total, these findings demonstrate that THY1 expression directly contributes to resistance to chemoradiation therapy.

### THY1 *expression in human GBM is spatial niche-dependent*

The *in vivo* studies suggesting that *THY1* expression is associated with therapeutic resistance and a mesenchymal gene expression signature, combined with recent studies suggesting that THY1+ cells often reside within a perivascular or stem cell niche and are associated with a mesenchymal and stem cell gene expression pattern [23,29], prompted us to evaluate the spatial distribution of *THY1* expressing cells in patient-derived GBM tumor tissue. We performed spatial quantitative whole transcriptome analyses (spatial transcriptomics) of image-guided intraoperative human GBM biopsies from a region of high perfusion(i.e., with high vascularity) which revealed that *THY1* expression significantly co-localized within the perivascular niche, characterized by co-expression of a glioma stem cell and mesenchymal signature, as well as TGF$\beta$ signaling (Figs. 6; S6A). We also performed spatial transcriptomics on a biopsy derived from a low perfusion region. This analysis also revealed that *THY1* was expressed within the perivascular niche and was significantly co-localized with a mesenchymal and stem cell signature and up-regulation of genes associated with TGF$\beta$ signaling (Figs. 6E, F; S6B). We then replicated these analyses utilizing image-guided biopsies from two additional treatment-naïve patients enrolled in our clinical study which further supported that THY1 cells co-localized within the perivascular niche with expression of a glioma stem cell and mesenchymal signature (Figs. 6G, S6C,D).

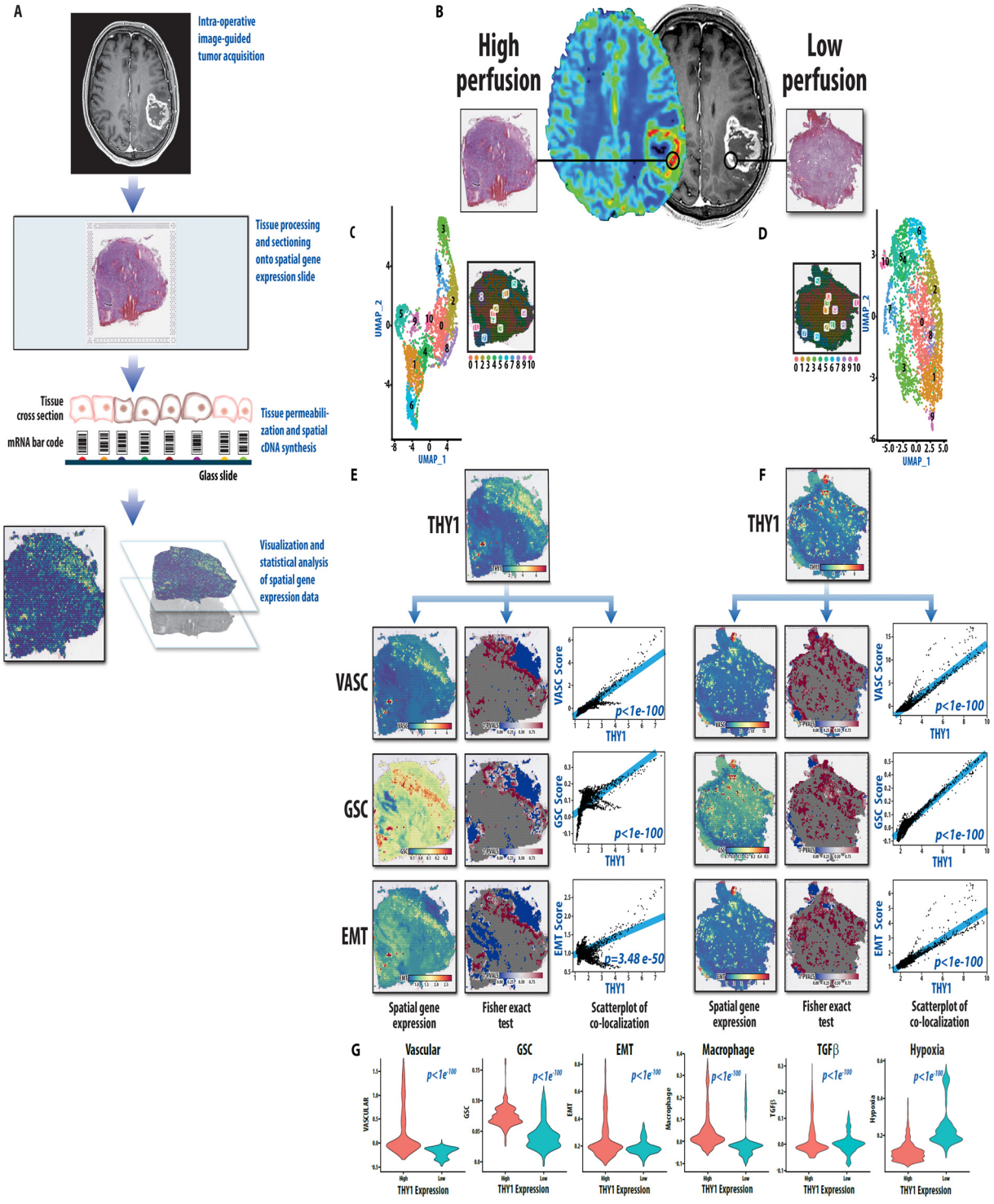


**Fig. 6.** Spatial transcriptomic analysis (ST) of treatment-naive human GBM biopsies reveal that *THY1* expression significantly co-localizes with a glioma stem cell (GSC), and epithelial to mesenchymal transition (EMT) gene expression signatures within the perivascular niche. (A) A schematic depicting the experimental approach for evaluating the spatial distribution of gene expression profiles within a GBM biopsy. (B) MRI from a patient with primary GBM showing T1-post contrast weighted MRI and corresponding perfusion (CBV) scan. Two image-guided stereotactic biopsies were acquired, one from a contrast-enhancing region with relative high-perfusion, and a second from an enhancing region with low-perfusion. (C,D) UMAP analyses depicting spatial regions with unique gene expression profiles within both samples. (E,F) ST analysis of a GBM biopsy from a region with high perfusion (E) and Low Perfusion (F). Spatial distribution of *THY1* expression is shown along with vascular (VASC), GSC, and EMT pathway enrichment scores. The left panels show the spatial gene expression of each individual gene set. The middle panel shows 1 minus p-values from a spatially local Fisher's exact test within each spot for significant overlap between regions with high pathway enrichment scores and high THY1 expression. Significance in spatial overlap between the pathway enrichment scores and *THY1* expression was tested by using a sliding window approach to perform spatially-local Fisher's test. On the right are scatterplots showing gene expression of *THY1*(x-axis) and enrichment scores for gene set of interest(y-axis) within each spatial location with line fitted. P-values show significance of correlation. *THY1* significantly co-localizes with these gene sets both in the high and low perfusion samples. (G) Violin plots evaluating spatial co-localization of THY1 high regions and THY1 low regions with gene sets of interest. The plots are a composite of ST spots from 4 clinical GBM samples from 3 patients, and show that *THY1* expression consistently co-localizes with vascular, GSC, EMT, macrophage, and TGF$\beta$ expression. Hypoxia shown as a negative comparison. p-values shown based on Student's t-test.

THY1 is a cell surface receptor whose physiologic function is the mediation of cell-cell communication [30–37]. Thus, to evaluate the cell types co-localizing with THY1+ GBM cells, we analyzed our spatial transcriptomic results of 4 samples from 3 patients which revealed that THY1 consistently co-localized with a macrophage gene expression profile ($p<1\times10^{-100}$) (Fig. S6). Tumor-associated macrophages are known to drive malignant growth, stem cell maintenance, and epithelial to mesenchymal transition (EMT) [3,38–41]. We then performed gene ontology pathway enrichment analyses for THY1 high vs low regions which revealed that cell adhesion and extracellular matrix pathways are highly upregulated in THY1-enriched regions both in the hypervascular (Fig. S7A,C) and hypovascular (Fig. S7B, D) samples, supporting our findings above (Fig. 2C). These data show that THY1+ cells consistently localize within a common tumor niche, suggesting a role for THY1 within the tumor microenvironment in a signaling axis that contributes to maintenance of a mesenchymal and cancer stem cell phenotype which contributes to treatment resistance.

## Discussion

Despite aggressive therapy for GBM with maximal safe resection and TMZ/IR, recurrence is inevitable, and therapeutically actionable mechanisms that drive resistance have yet to be identified. To characterize the molecular basis for the development of therapeutic resistance in GBM, we have developed and analyzed a pre-clinical *in vivo* recurrence model along with spatial analyses of patient-derived biopsies. A key finding from the described studies indicates that a rare population of pre-existing, therapy-resistant tumor cells within treatment-naïve GBM likely drive tumor recurrence. Specifically, this THY1+ cell population resides within a perivascular tumor niche strongly expressing EMT and stem cell genes, and co-localizes with macrophages. Our findings also suggest that tumor recurrence may be driven through critical cell-cell interactions, between THY1 expressing cells and macrophages, within the perivascular tumor microenvironment that drive a mesenchymal transition.

The GBM recurrence model that we have developed recapitulates the clinical treatment paradigm and results in profoundly resistant tumors at recurrence that emulate the pattern of recurrence clinically. Most notable was the finding that THY1 expression was increased greater than 100-fold in recurrent biopsies compared to pre-treatment biopsies. We then isolated, using THY1 as a cell surface marker, a population of cells from treatment-naïve tumors that recapitulated the treatment resistance phenotype of the recurrent tumor samples. Functional *in vitro* analyses revealed that experimentally induced THY1 overexpression resulted in increased treatment resistance, whereas ablation of THY1 expression using CRISPR/Cas9 mediated gene editing resulted in an increase in treatment sensitivity. The biological significance and clinical relevance of these results is further emphasized by the finding that THY1 expression is significantly upregulated in the majority of patients at the time of recurrence, and that increased THY1 expression was associated with worse overall survival. Although clonal selection of pre-existing therapy-resistant recurrence initiating cells in GBM has been described previously [8,42–44], the findings presented here provide a strong proof of the concept and identifies a specific phenotype and gene expression profile that characterizes this cell population.

Gene expression analysis of replicate paired pre-treatment and recurrent tumors from the same mouse revealed that development of a resistant phenotype was also associated with elevated expression of genes related to mesenchymal transition, stemness, cell adhesion and components of the extracellular matrix, as well as downregulation of genes associated with cell death. A mesenchymal gene expression signature results from the biological process of epithelial–mesenchymal transition (EMT) and is characterized by an enhanced capacity for invasion and metastasis in many malignancies [6,45–47]. Here we nominate THY1 as among the most significantly upregulated membrane proteins in cells acquiring a mesenchymal phenotype with properties of a recurrence initiating cell in GBM [20,21,23,24,34,36]. THY1 is a cell surface receptor that has been identified in several nonpathological cell types and is critical for cell-cell communication as well as cell-matrix interactions resulting in many physiological processes including proliferation, adhesion, and migration [20,34,36,48]. THY1 has been identified in several malignancies including renal cell cancers, breast cancer, hepatocellular carcinomas, ovarian cancer, and pancreatic tumors [29,34,48–52] and has been associated with invasion, metastasis, immune evasion, and poor prognosis, all of which are hallmarks of EMT.

In our paired *in vivo* analyses, the recurrent samples which had THY1 upregulation also had significantly increased expression of genes associated with cell morphogenesis, cell-cell contact, as well as cell adhesion and extracellular structure organization. These results were corroborated by our gene ontology pathway enrichment analyses of human GBM specimens (Fig. S6). These cellular pathways mediate signals for growth, migration, survival, differentiation, and resistance to cell death [53,54]. Avril *et al* demonstrated that THY1/CD90+ tumors have increased association with invasiveness and multi-focal tumor presentation [48]. These studies further support a role for THY1 in cell-cell communication and migration mediating treatment resistance.

Therapeutic resistance in glioblastoma is driven by marked inter- and intra-tumoral heterogeneity both at the cellular and microenvironmental level [3,7,55–57]. In the context of the tumor microenvironment (TME), distinct tumor niches, especially perivascular, hypoxic, and invasive tumor niches, have been shown to be enriched with therapy-resistant cancer stem cell populations [3,9,10,56–60]. These niches support resistant populations and play a critical role in tumor recurrence, as the interplay between the treatment refractory cells and adjacent cells including immune, stromal, differentiated cancer, glial, neuronal, and endothelial cells drives quiescence, invasion, immune suppression as well as other features promoting treatment resistance [3,61–63]. In order to target these stem-like, therapy-resistant cells, the signaling cascades that promote a resistant phenotype in the context of the local TME need to be better understood. The recently developed technique of spatial transcriptomics (ST) [64,65] provides the ability to interrogate whole transcriptome expression analysis *in situ*, permitting the assessment of the local tumor microenvironment. Due to the robust and reproducible evidence that THY1-positivity serves as a marker for a therapy resistant phenotype and hence may serve as a spatial landmark, we performed ST analyses of image-guided biopsies of a patient-derived GBM. This analysis was performed in an unsupervised and spatially-naïve manner and gene expression data was then superimposed onto the original H+E imaging. We found that in the analyses of hyper-perfused and hypo-perfused regions of a single GBM, THY1 expression consistently co-localized with a mesenchymal and stem-like signature and was found primarily in the perivascular niche [23], validating our studies in mouse models. Furthermore, our ST studies revealed co-localization of THY1 expression with a macrophage gene expression signature. Tumor-associated macrophages (TAMs) have been shown to maintain stem cell populations [3,38,55,66–69], and promote invasiveness and immune evasion through numerous interactions. For example, in breast cancer, TAMs were shown to preferentially infiltrate THY1+ regions, bind the THY1 receptor on cancer stem cells which resulted in juxtracrine signaling promoting invasiveness and supporting a stem cell niche, with activation of SRC and NF$\kappa$B signaling cascades [29]. These studies further revealed that depletion of macrophages resulted in arrest of tumor growth. In glioma, a recent study demonstrated that increased THY1 expression correlated with SRC phosphorylation, and resulted in a SRC-dependent tumor cell migration as well as cell-matrix interaction which was inhibited by the SRC-inhibitor, dasatinib [48]. Similarly, THY1+ mesenchymal stem cells have been shown to induce glioma progression through increasing tumor proliferation and cell migration [24]. Our data, in conjunction with existing literature, highlight the importance of cell-cell interactions within the TME in tumor progression and the critical role of THY1 in paracrine/juxtracrine signaling within its local niche.

Our preclinical and clinical studies also revealed upregulation of a mesenchymal gene expression profile with TGF$\beta$ pathway activation at recurrence. A number of studies have independently demonstrated a role for TGF$\beta$ signaling in treatment resistance [70–74], expression of stem cell markers, neurosphere formation ability as well as tumorigenic potential in mouse models [73,75,76]. Furthermore, inhibition of TGF$\beta$ signaling has been associated with a depletion of the stem cell population in breast cancer, leukemia and glioblastoma [75–79]. Our findings support this as inhibition of TGF$\beta$ signaling using LY2109761 decreased the expression of mesenchymal and stem-like genes. Interestingly, treatment of recurrent tumors with LY2109761 had minimal efficacy as single agent, however we observed an improved response when TMZ/IR was combined with TGFBR1 inhibition, suggesting a restoration of sensitivity to TMZ/IR. This finding directly implicates the TGF$\beta$ signaling pathway in imparting a mesenchymal, stem-like, therapy-resistant phenotype as previously described [79]. Recent clinical trials investigating various TGFBR inhibitors have not shown promise but have typically utilized TGFBR inhibitors alone or in combination with other drugs including lomustine [80,81]. However, our findings suggest that inhibition of the TGF$\beta$ signaling pathway may be most effective in a recurrent setting to reverse the resistance to TMZ/IR, especially if patients are enriched for the expression of a mesenchymal and stem-like signature described here. The specific pathway to resistance likely only occurs in a subpopulation of patients as evidenced by Wang *et al* who found mutations in LTBP4, a known activator of the TGF$\beta$ pathway, in 11% of patients at recurrence [8]. Therefore, identifying subgroups of patients who are likely to benefit from TGF$\beta$ targeting is critical [72]. Activation of the TGF$\beta$ signaling pathway and a mesenchymal phenotype is also associated with enhanced capacity to repair DNA damage thereby leading to chemo- and radiation-resistance through several transcription factors [82]. For example, ZEB2, which was upregulated in our recurrent samples, has been shown to affect ATM/ATR activity upon DNA damage [83]. Its homolog ZEB1, promotes radioresistance in breast cancer by regulating the stability of CHK1 and regulates TMZ sensitivity via regulation of MGMT in glioblastoma [84,85].

The development of recurrence is a dynamic process that is poorly understood. Many have theorized that the evolutionary pressure during treatment results in selection of clonal cells versus expansion and mutation of a subclonal population of cells [5,42,43,86]. Recently, Xie et al demonstrated that a subpopulation of quiescent GBM cancer stem cells evade treatment and proliferate leading to recurrence [87]. In agreement with this study and other recent reports, our findings demonstrate that evolution and growth of a pre-existing subclonal recurrence initiating tumor cell population can lead to recurrence [5,42,88].

In GBM, the most common site of tumor recurrence is often within the resection cavity or high-dose radiation field, rather than at more distant sites [89,90]. Although this suggests that resistant cell types often reside within the immediate surgical cavity and are the source of recurrence, the role distal infiltration plays in recurrence is not well-defined. Although tumors with high THY1 expression have been shown to be more invasive [48], whether these THY1+ tumor cells are a source of brain invasion in the immediate cavity is unknown and worthy of further study. Yet, given that we identified THY1+ cells with a mesenchymal and a recurrence initiating phenotype within the perivascular niche in pre-treatment tumors, and found notable upregulation of this cell type in recurrent tumors both in mice and in patients suggests that these cells are a source of local tumor recurrence.

In aggregate, our study provides a clinically relevant mouse model to study treatment resistance in GBM and defines a rare cell population expressing *THY1* that is intrinsically resistant to TMZ/IR therapy. It is critical to realize that the glioma stem cell hypothesis and its role in tumor recurrence is somewhat controversial. Furthermore, glioma stem cell markers are highly variable [91–93], and individual markers of stemness are not always reliable indicators of cancer stem cells. Here we have identified cells with a stem-like gene expression pattern that lead to recurrence with upregulation of mesenchymal pathways. These cells were identified by their expression of THY1 cell surface receptor which provided us with an opportunity to isolate and characterize them further.

Our mouse model approach provides a unique opportunity to explore mechanisms for tumor resistance and therapeutic interventions critical for patient care. Although *in vivo* immunocompromised murine models do not perfectly replicate the clinical paradigm or the human tumor microenvironment, our findings are validated by clinical findings. Furthermore, our human spatial transcriptomic analyses provide additional insights into interactions between human tumor cells and the tumor microenvironment. The use of patient-derived explants rather than immortalized cell lines in an intracranial mouse model to evaluate the evolution of resistance to combination therapy using a genome wide analysis of gene expression also provides confidence that our findings approximate the clinical setting. Consistent with clinical experience, our results demonstrate that adjuvant TMZ prolonged the overall survival from 7 weeks to 13 weeks. The development of recurrence in animals while undergoing adjuvant TMZ suggests that the tumors were truly resistant. In addition, the demonstration that resistance to TMZ/IR was recapitulated upon re-implantation of recurrent tumor tissues confirms this conclusion. Further efforts are needed to define how inherently resistant cells drive recurrence through interactions within the perivascular niche, which may lead to the identification of pathways to target for clinical benefit. In the recurrence model described here, we have utilized a combination of TMZ/IR to evaluate the mechanisms of treatment resistance. Although combination TMZ and IR is standard of care for GBM patients, a number of reports have tested the molecular basis for GBM resistance utilizing a single modality only [94,95], which although important, does not mimic the emergence of resistance in clinical settings.

## Author contributions

Conceptualization: W.N. Al-Holou., H. Wang, A.C. de Carvalho, T. Mikkelsen, A. Rehemtulla

Methodology: W.N. Al-Holou., H. Wang, V. Ravikumar, S. Shankar, M. Oneka, R.G.W. Verhaak, A. Rao, H. Kim, A. Rehemtulla

Investigation: W.N. Al-Holou, H. Wang, V. Ravikumar, S. Shankar, M. Oneka, R.G.W. Verhaak, H. Kim, Z. Fehmi, D.R. Wahl, S. Shankar, D. Pratt, S. Camelo-Piragua, A. Rao, C. Speers, A. Rehemtulla

Funding acquisition: W.N. Al-Holou, A.C. de Carvalho, T. Mikkelsen, A. Rao, A.Rehemtulla

Tissue and/or cell contribution: W.N. Al-Holou, A.C. de Carvalho, T. Mikkelsen, T. Hollon, O. Sagher, J.A. Heth, K.M. Muraszko

Writing – original draft: W.N. Al-Holou., H. Wang, V. Ravikumar, A. Rao, S. Shankar, M. Oneka, A. Rehemtulla

Writing – review & editing: W.N. Al-Holou., H. Wang, V. Ravikumar, M. Oneka, R.G.W. Verhaak, D.R. Wahl, S. Shankar, Z. Fehmi, D. Pratt, S. Camelo-Piragua, C. Speers, T. Hollon, O. Sagher, J.A. Heth, K.M. Muraszko, T.S. Lawrence, A.C. de Carvalho, T. Mikkelsen, A. Rao, A. Rehemtulla

## Funding

Research reported in this publication was supported by National Institute of Health(NIH) grants P01-CA085878 and 5R01CA241764. Research was supported by the National Cancer Institute (NCI) of the NIH under award number P30CA046592. M.O. V.R., and A. Rao were supported by National Cancer Institute (NCI) R37CA214955, a gift from Agilent Technologies, a University of Michigan MIDAS PODS Grant, and a Research Scholar Grant from the American Cancer Society (RSG-16-005-01). Research was also supported by the Department of Defense (CA180174), the NIH/Michigan Institute for Clinical and Health Research (UL1TR002240), the Congress of Neurological Surgeons Tumor fellowship, the American Brain Tumor Association, and the Christina Costa Brain Tumor Research Fund.

## Declaration of Competing Interest

The authors declare that they have no known competing financial interests or personal relationships that could have appeared to influence the work reported in this paper.

## Acknowledgments

Tumor specimens obtained from the University of Michigan were obtained through the CNS Tissue Biorepository (HUM00024610) and the Henry Ford brain tumor center. We would like to thank Steven Kronenberg for assistance with editing and illustration of figures. The results shown here are in part based upon data generated by the TCGA Research Network: https://www.cancer.gov/tcga, and the Glass Consortium (https://www.glass-consortium.org/). We would also like to thank Kait Verbal for her assistance in acquiring tumor samples through the CNS Tissue Biorepository. We would like to thank Dah-Luen Huang, Pavlina Zafirovska, Susan Dagenais, Judy Opp, Ingrid Bergin, and Olivia Koues for assistance in processing our ST samples. We would also like to thank Kamlai Saiya-Cork from the University of Michigan Flow Cytometry Core for assistance in processing our flow cytometry samples.

## Supplementary materials

Supplementary material associated with this article can be found, in the online version, at doi:10.1016/j.neo.2022.100872.

## References

[1] R. Stupp, et al., Effects of radiotherapy with concomitant and adjuvant temozolomide versus radiotherapy alone on survival in glioblastoma in a randomised phase III study: 5-year analysis of the EORTC-NCIC trial, Lancet Oncol. 10 (5) (2009) 459–466.
[2] R. Stupp, et al., Radiotherapy plus concomitant and adjuvant temozolomide for glioblastoma, N. Engl. J. Med. 352 (10) (2005) 987–996.
[3] D. Hambardzumyan, G. Bergers, Glioblastoma: defining tumor niches, Trends Cancer 1 (4) (2015) 252–265.
[4] N.R. Parker, et al., Intratumoral heterogeneity identified at the epigenetic, genetic and transcriptional level in glioblastoma, Sci. Rep. 6 (2016) 22477.
[5] H. Kim, et al., Whole-genome and multisector exome sequencing of primary and post-treatment glioblastoma reveals patterns of tumor evolution, Genome Res. 25 (3) (2015) 316–327.
[6] R.G.W. Verhaak, et al., Integrated genomic analysis identifies clinically relevant subtypes of glioblastoma characterized by abnormalities in PDGFRA, IDH1, EGFR, and NF1, Cancer Cell 17 (1) (2010) 98–110.
[7] S. Osuka, E.G. Van Meir, Overcoming therapeutic resistance in glioblastoma: the way forward, J. Clin. Invest. 127 (2) (2017) 415–426.
[8] J. Wang, et al., Clonal evolution of glioblastoma under therapy, Nat. Genet. 48 (7) (2016) 768–776.
[9] J.D. Lathia, et al., Deadly teamwork: neural cancer stem cells and the tumor microenvironment, Cell Stem Cell 8 (5) (2011) 482–485.
[10] A. Bronisz, et al., Hypoxic roadmap of glioblastoma-learning about directions and distances in the brain tumor environment, Cancers 12 (5) (2020) (Basel).
[11] J.D. Lathia, et al., Cancer stem cells in glioblastoma, Genes Dev. 29 (12) (2015) 1203–1217.
[12] X. Lan, et al., Fate mapping of human glioblastoma reveals an invariant stem cell hierarchy, Nature 549 (7671) (2017) 227–232.
[13] A.D. Berezovsky, et al., Sox2 promotes malignancy in glioblastoma by regulating plasticity and astrocytic differentiation, Neoplasia 16 (3) (2014) 193–206 206 e19-25.
[14] L.F. Ye, et al., Patient-derived glioblastoma cultures as a tool for small-molecule drug discovery, Oncotarget 11 (4) (2020) 443–451.
[15] S. Galban, et al., MRI-guided stereotactic biopsy of murine GBM for spatiotemporal molecular genomic assessment, Tomography 3 (1) (2017) 9–15.
[16] F. Jacob, et al., A patient-derived glioblastoma organoid model and biobank recapitulates inter- and intra-tumoral heterogeneity, Cell 180 (1) (2020) 188-204 e22.
[17] G. Consortium, Glioma through the looking GLASS: molecular evolution of diffuse gliomas and the glioma longitudinal analysis consortium, Neuro-Oncol. 20 (7) (2018) 873–884.
[18] A. Balbous, et al., A mesenchymal glioma stem cell profile is related to clinical outcome, Oncogenesis 3 (2014) e91.
[19] S. Lamouille, J. Xu, R. Derynck, Molecular mechanisms of epithelial-mesenchymal transition, Nat. Rev. Mol. Cell Biol. 15 (3) (2014) 178–196.
[20] J.E. Bradley, G. Ramirez, J.S. Hagood, Roles and regulation of Thy-1, a context-dependent modulator of cell phenotype, Biofactors 35 (3) (2009) 258–265.
[21] T. Shahar, et al., Percentage of mesenchymal stem cells in high-grade glioma tumor samples correlates with patient survival, Neuro. Oncol. 19 (5) (2017) 660–668.
[22] A. Kramer, et al., Causal analysis approaches in ingenuity pathway analysis, Bioinformatics 30 (4) (2014) 523–530.
[23] J. He, et al., CD90 is identified as a candidate marker for cancer stem cells in primary high-grade gliomas using tissue microarrays, Mol. Cell. Proteomics 11 (6) (2012) M111 010744.
[24] Q. Zhang, et al., CD90 determined two subpopulations of glioma-associated mesenchymal stem cells with different roles in tumour progression, Cell Death Dis. 9 (11) (2018) 1101.
[25] S.G. Zhao, et al., Xenograft-based, platform-independent gene signatures to predict response to alkylating chemotherapy, radiation, and combination therapy for glioblastoma, Neuro-Oncol. 21 (9) (2019) 1141–1149.
[26] A. Murat, et al., Stem cell-related "self-renewal" signature and high epidermal growth factor receptor expression associated with resistance to concomitant chemoradiotherapy in glioblastoma, J. Clin. Oncol. 26 (18) (2008) 3015–3024.
[27] A. Schulte, et al., A distinct subset of glioma cell lines with stem cell-like properties reflects the transcriptional phenotype of glioblastomas and overexpresses CXCR4 as therapeutic target, Glia 59 (4) (2011) 590–602.
[28] J. van den Boom, et al., Characterization of gene expression profiles associated with glioma progression using oligonucleotide-based microarray analysis and real–time reverse transcription-polymerase chain reaction, Am. J. Pathol. 163 (3) (2003) 1033–1043.
[29] H. Lu, et al., A breast cancer stem cell niche supported by juxtacrine signalling from monocytes and macrophages, Nat. Cell Biol. 16 (11) (2014) 1105–1117.
[30] A.M. Avalos, et al., Aggregation of integrins and RhoA activation are required for Thy-1-induced morphological changes in astrocytes, J. Biol. Chem. 279 (37) (2004) 39139–39145.
[31] A.M. Avalos, et al., Neuronal Thy-1 induces astrocyte adhesion by engaging syndecan-4 in a cooperative interaction with alphavbeta3 integrin that activates PKCalpha and RhoA, J. Cell Sci. 122 (Pt 19) (2009) 3462–3471.
[32] L. Leyton, et al., Thy-1 binds to integrin beta(3) on astrocytes and triggers formation of focal contact sites, Curr. Biol. 11 (13) (2001) 1028–1038.
[33] R.V.A.K.M. Herrera-Molina, A. Alvarez, A. Cardenas, A.F.G. Quest, L. Leyton, International review of cell and molecular biology. Volume three hundred and three, Int. Rev. Cell Mol. Biol. 305 (2013) Amsterdam; Boston: Elsevier/AP. 410 pages.
[34] C. Sauzay, et al., CD90/Thy-1, a cancer-associated cell surface signaling molecule, Front. Cell Dev. Biol. 7 (2019) 66.
[35] W.S. Lee, et al., Thy-1, a novel marker for angiogenesis upregulated by inflammatory cytokines, Circ. Res. 82 (8) (1998) 845–851.
[36] L. Leyton, et al., Thy-1/CD90 a bidirectional and lateral signaling scaffold, Front. Cell Dev. Biol. 7 (2019) 132.
[37] P. Hu, et al., Thy-1-integrin interactions in cis and trans mediate distinctive signaling, Front. Cell Dev. Biol. 10 (2022) 928510.
[38] D. Hambardzumyan, D.H. Gutmann, H. Kettenmann, The role of microglia and macrophages in glioma maintenance and progression, Nat. Neurosci. 19 (1) (2016) 20–27.
[39] A. Wu, et al., Glioma cancer stem cells induce immunosuppressive macrophages/microglia, Neuro-Oncol. 12 (11) (2010) 1113–1125.
[40] W. Zhou, et al., Periostin secreted by glioblastoma stem cells recruits M2 tumour-associated macrophages and promotes malignant growth, Nat. Cell Biol. 17 (2) (2015) 170–182.
[41] E. Gangoso, et al., Glioblastomas acquire myeloid-affiliated transcriptional programs via epigenetic immunoediting to elicit immune evasion, Cell 184 (9) (2021) 2454-2470 e26.
[42] D. Chowell, et al., Modeling the subclonal evolution of cancer cell populations, Cancer Res. 78 (3) (2018) 830–839.
[43] L. Ding, et al., Clonal evolution in relapsed acute myeloid leukaemia revealed by whole-genome sequencing, Nature 481 (7382) (2012) 506–510.
[44] T. Mazor, et al., DNA methylation and somatic mutations converge on the cell cycle and define similar evolutionary histories in brain tumors, Cancer Cell 28 (3) (2015) 307–317.
[45] K.P. Bhat, et al., Mesenchymal differentiation mediated by NF-kappaB promotes radiation resistance in glioblastoma, Cancer Cell 24 (3) (2013) 331–346.
[46] Y. Piao, et al., Acquired resistance to anti-VEGF therapy in glioblastoma is associated with a mesenchymal transition, Clin. Cancer Res. 19 (16) (2013) 4392–4403.
[47] W.Y. Cheng, et al., A multi-cancer mesenchymal transition gene expression signature is associated with prolonged time to recurrence in glioblastoma, PLoS One 7 (4) (2012) e34705.
[48] T. Avril, et al., CD90 expression controls migration and predicts dasatinib response in glioblastoma, Clin. Cancer Res. 23 (23) (2017) 7360–7374.
[49] B. Bussolati, et al., Identification of a tumor-initiating stem cell population in human renal carcinomas, FASEB J. 22 (10) (2008) 3696–3705.
[50] L. Zhu, et al., Evidence of CD90+CXCR4+ cells as circulating tumor stem cells in hepatocellular carcinoma, Tumour Biol. 36 (7) (2015) 5353–5360.
[51] Z.F. Yang, et al., Significance of CD90+ cancer stem cells in human liver cancer, Cancer Cell 13 (2) (2008) 153–166.
[52] V.S. Donnenberg, et al., Localization of CD44 and CD90 positive cells to the invasive front of breast tumors, Cytometry B Clin. Cytom. 78 (5) (2010) 287–301.
[53] R. Schmidmaier, P. Baumann, ANTI-ADHESION evolves to a promising therapeutic concept in oncology, Curr. Med. Chem. 15 (10) (2008) 978–990.
[54] R. Kalluri, R.A. Weinberg, The basics of epithelial-mesenchymal transition, J. Clin. Invest. 119 (6) (2009) 1420–1428.
[55] B.C. Prager, et al., Glioblastoma stem cells: driving resilience through chaos, Trends Cancer 6 (3) (2020) 223–235.

[56] S. Seidel, et al., A hypoxic niche regulates glioblastoma stem cells through hypoxia inducible factor 2 alpha, Brain 133 (Pt 4) (2010) 983–995.
[57] D.L. Schonberg, et al., Brain tumor stem cells: molecular characteristics and their impact on therapy, Mol. Aspects Med. 39 (2014) 82–101.
[58] D. Schiffer, et al., Glioblastoma: microenvironment and niche concept, Cancers 11 (1) (2018) (Basel).
[59] J.D. Lathia, et al., Integrin alpha 6 regulates glioblastoma stem cells, Cell Stem Cell 6 (5) (2010) 421–432.
[60] H. Ruiz-Garcia, et al., Engineering three-dimensional tumor models to study glioma cancer stem cells and tumor microenvironment, Front. Cell Neurosci. 14 (2020) 558381.
[61] X. Wang, et al., Reciprocal signaling between glioblastoma stem cells and differentiated tumor cells promotes malignant progression, Cell Stem Cell 22 (4) (2018) 514-528 e5.
[62] M. Jamal, et al., Microenvironmental regulation of glioblastoma radioresponse, Clin. Cancer Res. 16 (24) (2010) 6049–6059.
[63] M. Jamal, et al., The brain microenvironment preferentially enhances the radioresistance of CD133(+) glioblastoma stem-like cells, Neoplasia 14 (2) (2012) 150–158.
[64] E. Berglund, et al., Spatial maps of prostate cancer transcriptomes reveal an unexplored landscape of heterogeneity, Nat. Commun. 9 (1) (2018) 2419.
[65] S. Maniatis, et al., Spatiotemporal dynamics of molecular pathology in amyotrophic lateral sclerosis, Science 364 (6435) (2019) 89–93.
[66] X.Z. Ye, et al., Tumor-associated microglia/macrophages enhance the invasion of glioma stem-like cells via TGF-beta1 signaling pathway, J. Immunol. 189 (1) (2012) 444–453.
[67] T. Hara, et al., Interactions between cancer cells and immune cells drive transitions to mesenchymal-like states in glioblastoma, Cancer Cell 39 (6) (2021) 779-792 e11.
[68] C. Lee-Chang, et al., Myeloid-derived suppressive cells promote B cell-mediated immunosuppression via transfer of PD-L1 in glioblastoma, Cancer Immunol. Res. 7 (12) (2019) 1928–1943.
[69] A.L. Chang, et al., CCL2 produced by the glioma microenvironment is essential for the recruitment of regulatory T cells and myeloid-derived suppressor cells, Cancer Res. 76 (19) (2016) 5671–5682.
[70] S.A. Mani, et al., The epithelial-mesenchymal transition generates cells with properties of stem cells, Cell 133 (4) (2008) 704–715.
[71] K. Polyak, R.A. Weinberg, Transitions between epithelial and mesenchymal states: acquisition of malignant and stem cell traits, Nat. Rev. Cancer 9 (4) (2009) 265–273.
[72] N.S. Bayin, et al., Patient-specific screening using high-grade glioma explants to determine potential radiosensitization by a TGF-beta small molecule inhibitor, Neoplasia 18 (12) (2016) 795–805.
[73] M.E. Hardee, et al., Resistance of glioblastoma-initiating cells to radiation mediated by the tumor microenvironment can be abolished by inhibiting transforming growth factor-beta, Cancer Res. 72 (16) (2012) 4119–4129.
[74] N. Oshimori, D. Oristian, E. Fuchs, TGF-beta promotes heterogeneity and drug resistance in squamous cell carcinoma, Cell 160 (5) (2015) 963–976.
[75] H. Ikushima, et al., Autocrine TGF-beta signaling maintains tumorigenicity of glioma-initiating cells through Sry-related HMG-box factors, Cell Stem Cell 5 (5) (2009) 504–514.
[76] J. Anido, et al., TGF-beta receptor inhibitors target the CD44(high)/Id1(high) Glioma-Initiating Cell Population in Human Glioblastoma, Cancer Cell 18 (6) (2010) 655–668.
[77] K. Naka, et al., TGF-beta-FOXO signalling maintains leukaemia-initiating cells in chronic myeloid leukaemia, Nature 463 (7281) (2010) 676–680.
[78] M. Shipitsin, et al., Molecular definition of breast tumor heterogeneity, Cancer Cell 11 (3) (2007) 259–273.
[79] M. Zhang, et al., Trimodal glioblastoma treatment consisting of concurrent radiotherapy, temozolomide, and the novel TGF-beta receptor I kinase inhibitor LY2109761, Neoplasia 13 (6) (2011) 537–549.
[80] A.A. Brandes, et al., A Phase II randomized study of galunisertib monotherapy or galunisertib plus lomustine compared with lomustine monotherapy in patients with recurrent glioblastoma, Neuro. Oncol. 18 (8) (2016) 1146–1156.
[81] U. Bogdahn, et al., Targeted therapy for high-grade glioma with the TGF-beta2 inhibitor trabedersen: results of a randomized and controlled phase IIb study, Neuro. Oncol. 13 (1) (2011) 132–142.
[82] M.H. Barcellos-Hoff, F.A. Cucinotta, New tricks for an old fox: impact of TGFbeta on the DNA damage response and genomic stability, Sci. Signal 7 (341) (2014) re5.
[83] A.E. Sayan, et al., SIP1 protein protects cells from DNA damage-induced apoptosis and has independent prognostic value in bladder cancer, Proc. Nat. Acad. Sci. U.S.A. 106 (35) (2009) 14884–14889.
[84] P. Zhang, et al., ATM-mediated stabilization of ZEB1 promotes DNA damage response and radioresistance through CHK1, Nat. Cell Biol. 16 (9) (2014) 864–875.
[85] F.A. Siebzehnrubl, et al., The ZEB1 pathway links glioblastoma initiation, invasion and chemoresistance, EMBO Mol. Med. 5 (8) (2013) 1196–1212.
[86] M.R. Blomquist, et al., Temporospatial genomic profiling in glioblastoma identifies commonly altered core pathways underlying tumor progression, Neurooncol Adv 2 (1) (2020) vdaa078.
[87] X.P. Xie, et al., Quiescent human glioblastoma cancer stem cells drive tumor initiation, expansion, and recurrence following chemotherapy, Dev. Cell 57 (1) (2022) 32-46 e8.
[88] R. Reinartz, et al., Functional Subclone profiling for prediction of treatment-induced intratumor population shifts and discovery of rational drug combinations in human glioblastoma, Clin. Cancer Res. 23 (2) (2017) 562–574.
[89] A.A. Brandes, et al., Recurrence pattern after temozolomide concomitant with and adjuvant to radiotherapy in newly diagnosed patients with glioblastoma: correlation With MGMT promoter methylation status, J. Clin. Oncol. 27 (8) (2009) 1275–1279.
[90] B.J. Gebhardt, et al., Patterns of failure for glioblastoma multiforme following limited-margin radiation and concurrent temozolomide, Radiat. Oncol. 9 (2014) 130.
[91] A. Bhaduri, et al., Outer radial glia-like cancer stem cells contribute to heterogeneity of glioblastoma, Cell Stem Cell 26 (1) (2020) 48-63 e6.
[92] D.V. Brown, et al., Expression of CD133 and CD44 in glioblastoma stem cells correlates with cell proliferation, phenotype stability and intra-tumor heterogeneity, PLoS One 12 (2) (2017) e0172791.
[93] P. Brescia, C. Richichi, G. Pelicci, Current strategies for identification of glioma stem cells: adequate or unsatisfactory? J. Oncol. (2012) 376894 2012.
[94] G.J. Kitange, et al., Inhibition of histone deacetylation potentiates the evolution of acquired temozolomide resistance linked to MGMT upregulation in glioblastoma xenografts, Clin. Cancer Res. 18 (15) (2012) 4070–4079.
[95] T.C. Johannessen, R. Bjerkvig, Molecular mechanisms of temozolomide resistance in glioblastoma multiforme, Expert Rev. Anticancer Ther. 12 (5) (2012) 635–642.
[96] S.G. Zhao, et al., Xenograft-based, platform-independent gene signatures to predict response to alkylating chemotherapy, radiation, and combination therapy for glioblastoma, Neuro-Oncol. 21 (9) (2019) 1141–1150.